Scripta Materialia 141 (2017) 32–35

Contents lists available at ScienceDirect

Scripta Materialia

journal homepage: www.elsevier.com/locate/scriptamat

Regular article

Effect of strut orientation on the microstructure heterogeneities in AlSi10Mg lattices processed by selective laser melting

Pauline Delroisse [a], Pascal J. Jacques [a], Eric Maire [b], Olivier Rigo [c], Aude Simar [a,*,1]

[a] Institute of Mechanics, Materials and Civil Engineering (iMMC), Université catholique de Louvain, 1348 Louvain-la-Neuve, Belgium
[b] MATEIS UMR5510, Institut National des Sciences Appliquées de Lyon (INSA), 69621 Villeurbanne, France
[c] Sirris, ADD Group, 4102 Seraing, Belgium

ARTICLE INFO

Article history:
Received 6 July 2017
Received in revised form 19 July 2017
Accepted 19 July 2017
Available online xxxx

Keywords:
Aluminum alloys
Rapid solidification
Three-dimensional tomography
Coarsening
Selective laser melting

ABSTRACT

The microstructure heterogeneities are compared between inclined and vertical struts of AlSi10Mg lattices processed by Selective Laser Melting. While the vertical struts present a fully dense homogenous microstructure, large levels of porosities and heterogeneous microstructure are present in inclined struts, particularly a much larger level of porosities in the bottom part of the strut compared to the top part. These differences are due to a larger time spent at high temperature for the bottom zone of the strut. A solutionizing and aging heat treatment homogenizes the microstructure but leads to a minor softening due to eutectic spheroidization.

Additive manufacturing (AM) of metallic parts is increasingly considered as a viable manufacturing process for industrial sectors with stringent quality criteria. More specifically, this recent technology attracts increasing interest in aerospace applications since it allows free design of complex parts like lattice structures [1–2]. The Selective Laser Melting (SLM) technology is an AM technology consisting in the layer-by-layer local melting of a metallic powder by a laser heat source [2–4].

AlSi10Mg is a hypoeutectic aluminum alloy widely used in SLM [3–4]. The microstructure of AlSi10Mg parts processed by SLM is much finer compared to cast parts of the same alloy [4–7] due to a much faster solidification rate (~10^6 °C/s) [5,8]. Since hardness increases with increasing microstructure refinement, AlSi10Mg processed by SLM present a higher hardness (~127 HV) than in the case of processing by high pressure casting (~ 100 HV) [5]. Furthermore, the microstructure cell size in the SLM process is heterogeneous at the scale of one melt pool [4–5,9]. The core of the melt pool exhibits the finest size of cells composed of the primary α-Al phase and the Si-rich eutectic (~0.4 [5]). The boundaries of the melt pool present a coarser microstructure as large as 0.8 μm [5] due to the longer time at high temperature. The specific study of the microstructure size and particularities in these zones has been widely investigated in AlSi10Mg SLM bulk samples [4–5,7,10].

Another important parameter affecting the microstructure is the spatial location dependency, in particular in orientated parts. Hitzler et al. [11] determined different levels of microstructure refinement as a function of the orientation with respect to the building direction. As far as thin structures (such as struts of lattice materials) are concerned, hardly anything has been reported about the microstructure evolution with the strut orientation relative to the building direction [1,12–13]. Similarly to bulk samples, the three different regions of the melt pool were observed [1,13]. Moreover, Qiu et al. [12] identified optimized parameters to process lattice structures by SLM with a porosity level below 1%. However, Qiu et al. [12] only observed one specific location of the lattice sample. It is thus worth noting that none of these studies have evidenced the combined influence of the strut orientation and spatial location (upwards or downwards orientated part) on the microstructure and porosity. The present study thus aims at demonstrating the very specific micro- and meso-structures resulting from SLM processing of fine AlSi10Mg struts.

In the present study, lattice structures with a built strut diameter of 820 μm presenting two different building orientations have been compared (Fig. 1): one referred to as the "vertical" strut (a) and one referred to as the "inclined" strut, orientated at 35.5° from horizontal plane (b). This orientation of the strut corresponds to the one of struts in a body centred cubic (BCC) unit cell of a lattice structure. The analyzed struts were thus part of a larger lattice structure to avoid border effects. The aluminum alloy contains 9.53 wt% of Si and 0.36 wt% of Mg. The powder particles size before laser melting ranged from 10 to 80 μm with a median value of 44 μm. The processing parameters of the SLM 250

* Corresponding author.
E-mail address: aude.simar@uclouvain.be (A. Simar).
[1] Postal address: Place Sainte Barbe 2/L5.02.02, 1348 Louvain-La-Neuve, Belgium.

http://dx.doi.org/10.1016/j.scriptamat.2017.07.020
1359-6462/

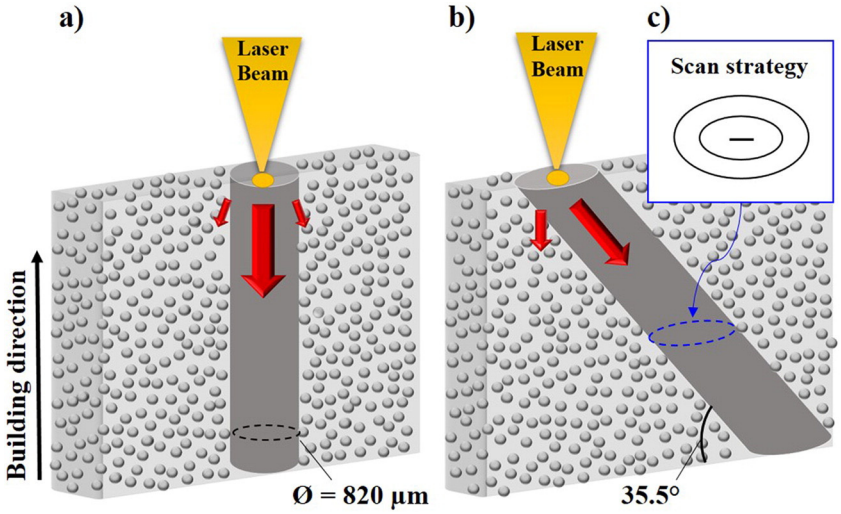

Fig. 1. Schematic representation of (a) the vertical, (b) the inclined struts and (c) the scan strategy. The red arrows indicate the thermal flux density and direction. (For interpretation of the references to color in this figure legend, the reader is referred to the web version of this article.)

equipment were a laser power of 250 W, a scanning speed of 571 mm/s, a layer thickness of 60 µm and an argon gas atmosphere. These process parameters were shown to bring low porosity in vertical struts and were voluntarily kept identical for all struts, whatever their building direction in order to assess the consequences on the microstructure and porosity. Because of the thin diameter of the struts, only two concentric round melting paths with a central strip were applied to build a strut section, with a following distance between each path of 0.15 mm (Fig. 1(c)).

The microstructure was investigated by light microscopy to highlight the melt pools while Scanning Electron Microscopy (SEM) was used to characterize the microstructure at higher magnification. Chemical etching with a Flick's reagent [14] revealed the Si-rich eutectic structure. SEM image analysis and 3D X-ray microtomography [15] were used to characterize the internal porosity of the struts. In this last case, the voxel size was set to 0.8 μm^3 with operating voltage of 80 kV and current of 280 µA without filtering. It is worth noting that Archimede's density measurement method is not well adapted to such small samples according to standard EN 623-2. The hydrogen content after SLM processing was estimated by alloy melting and released gas analysis. Vickers micro-hardness measurements were carried out on polished samples before the final etching step. At least 10 indents (15 g during 10 s) were performed on each sample to provide sufficient statistics.

Fig. 2 illustrates the microstructure of an inclined strut. Two different zones partitioned by the red dashed line are distinguishable. Zone A presents a fine microstructure characterized by small cells of primary Al surrounded by the Si rich eutectic phase. The usual arc-shaped melt pools are also clearly visible. Zone B, at the bottom, presents a coarser microstructure than zone A. The sample cell size measured by the mean linear intercept method in the core of the melt pools in both zones is given in Table 1. The inter-eutectic cells are roughly 2.5 to 3

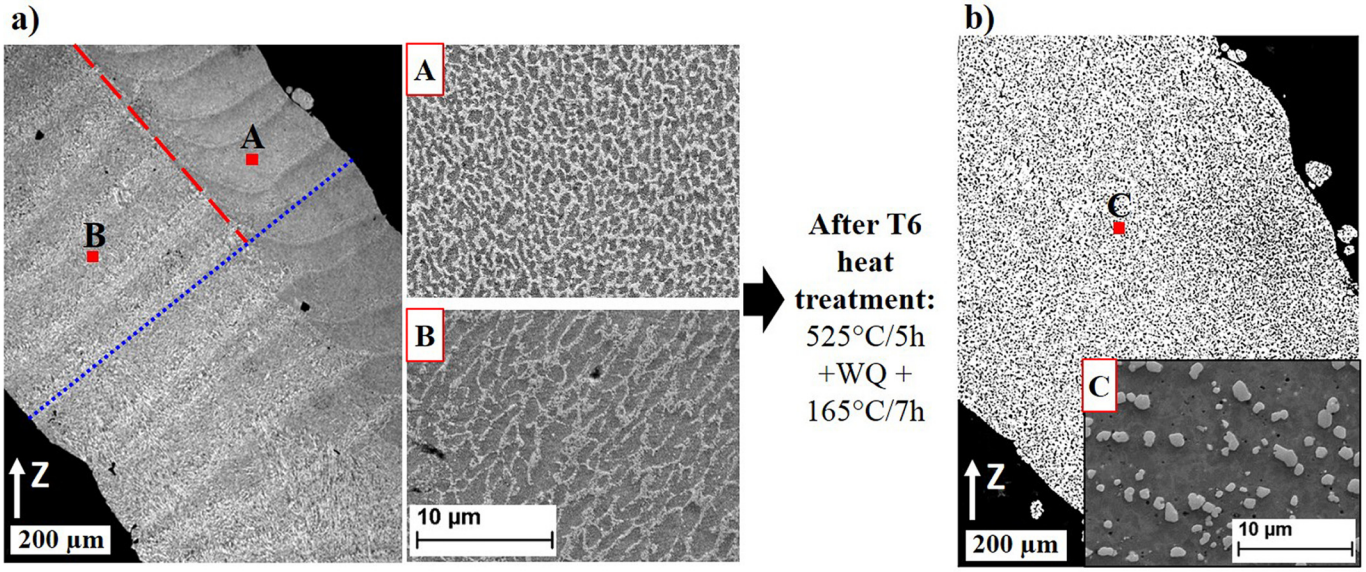

Fig. 2. Light and SEM (zoom) micrographs of the microstructure in an inclined strut. (a) Upper zone A presents a fine microstructure while lower zone B presents a coarser cellular dendritic microstructure. The blue dotted line is the cut plane for Fig. 3. (b) Homogenized microstructure after a T6 heat treatment (525°/5 h + water quenching (WQ) + 165°/7 h). (For interpretation of the references to color in this figure legend, the reader is referred to the web version of this article.)

Table 1
Microstructure cell size and Vickers hardness measured in the XY plane of vertical and oriented struts (zones A and B of Figs. 2 and 3).

	Microstructure cell size [μm]		Hardness [HV]	
Vertical strut	0.45 ± 0.23		124.9 ± 7.6	
Inclined strut	Zone A	Zone B	Zone A	Zone B
	0.45 ± 0.24	1.44 ± 0.81	120.6 ± 4.5	106.1 ± 3.4

times thinner in zone A of the orientated strut than in zone B. These two distinctive zones A and B are found on every inclined strut of the lattice structure.

To confirm the spatial influence of the strut orientation with respect to the building direction on the resulting microstructure, cross-sections of the inclined and vertical struts are compared in Fig. 3. The microstructure of the vertical strut is much more homogeneous with only the usual melt pool boundaries.

The existence of two distinct microstructural zones in the inclined strut (Fig. 2) can be explained by the influence of the orientation with respect to the building direction on the cooling conditions after melting. Generally, three heat loss phenomena define the thermal history, radiation, convection and conduction. In the present case, the radiation and convection processes are assumed to be constant since each sample section is constant and built similarly. Consequently, the major part of heat injected in the successive melt pools is transferred and evacuated by conduction in two directions: (i) towards the previous lower layers which have already cooled down, (ii) towards the unmelted surrounding powder bed. Obviously, the heat losses by conduction are influenced by the sample geometry. As depicted by the red arrows in Fig. 1, the thermal behavior (density and direction) differs during SLM process according to the building orientation and leads to solidification rate specific to each geometry [16]. Compared to the vertical strut, the inclined strut presents two zones with different thermal conductivities: the bottom zone, also called downwards orientated zone (DOZ) (zone B – Fig. 2), laying on support layers made of previous unmelted powder and the top zone (upwards orientated zone (UOZ)(zone A – Fig. 2), laying on dense material. The DOZ thus cools down more slowly than the UOZ since the powder acts as a thermal insulator and keeps the last layer longer at high temperature [8,16]. This difference of the cooling rate with the spatial location explains the difference in size of the cells between both zones. Indeed, a larger cooling rate avoids microstructure coarsening. Consequently, the mean size of the cells is roughly 2.5 to 3 times smaller in zone A and comparable to the 0.55 μm cell size measured in bulk AlSi10Mg samples presenting the same process parameters.

Moreover, it appears that the cell size in the core of the melt pool of the vertical struts is similar to zone A of the inclined strut due to the vertical building direction of these struts. The thermal flux density and orientation are indicated by the red arrows in Fig. 1. The successive layers always lay on dense material (except for the first one) and cool down faster by conduction just like in zone A of the inclined strut. As a consequence of these cell sizes, hardness measurements performed in the center of the melt pool in parts A and B of the inclined strut and in the vertical strut are compared in Table 1. The hardness is about 14 HV larger in the fine cell size zone A (UOZ) than in the DOZ of the inclined strut. The vertical strut presents only a slightly higher hardness than zone A of the inclined strut consistent with the similar cell size in these two samples.

As a consequence of the specific building process, the relative density was also investigated owing to X-ray microtomography. Fig. 3 shows that the porosity level is low for vertical strut. It was estimated at 0.4% by image analysis, which is a similar level to the porosity reported by Qiu et al. [12] for optimized fine AlSi10Mg struts. Furthermore, this level is slightly larger than in zone A of the inclined strut (0.1%). On the contrary, zone B is much highly porous (3.7%). Two virtual vertical parallelepipeds extracted from microtomography in zones A and B of the inclined strut are shown in Fig. 3(c). The porosity levels are 0.1% and 4.0% in zone A and B respectively, i.e. more than one order of magnitude difference between zones A and B, whatever the analysis method (SEM or tomography). Note that a thinner strut (diameter 600 μm) has also been analyzed by X-ray tomography. Again, an order of magnitude difference in porosity was found between the two zones, i.e. 0.25% of porosity in the UOZ compared to 2.7% in the DOZ. As largely discussed in the literature on bulk materials [17–19], porosities in aluminum alloys processed by SLM are expected to partly result from hydrogen content in the powder. In the present study, the total hydrogen content (on the surface, entrapped and/or dissolved) in the powder material and in the inclined strut were measured to be 27.4 ppm and 27.0 ppm, respectively, i.e. very similar. Considering the hydrogen as an ideal gas at room temperature, this corresponds to 35 mL/100 g.

Generally, spherical pores in SLM techniques are due to powder contamination and manufacturing issues. Indeed, their origins can be attributed to two phenomena: degassed and trapped hydrogen [17–19] and/or argon bubbled chamber gas [19]. The big surface over volume ratio of the powder particles increases their contamination risk with external elements.

In the case of AlSi10Mg processed by SLM, Weingarten et al. [17] observed that 96% of the porosities contain hydrogen. Indeed, moisture in the powder particles is the main reason for the formation of hydrogen porosity [17]. During the SLM process, this moisture reacts with the

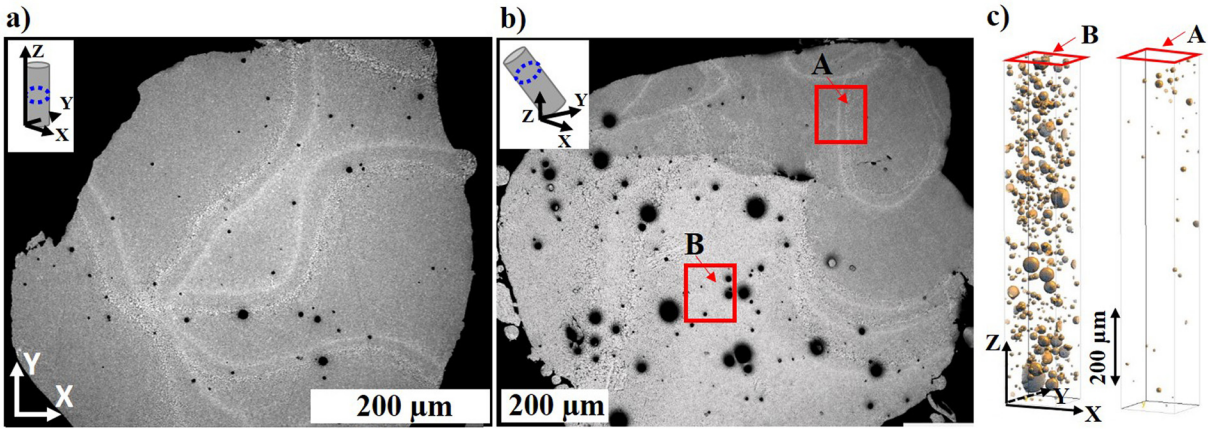

Fig. 3. Comparison of the microstructure of (a) a vertical and (b) an inclined strut. The orientation of the observation plane is given by the blue dotted line (see also Fig. 2). (c) Porosity in zone A and B of (b) observed by 3D X-ray tomography along virtual parallelepiped oriented along the axis of the strut. (For interpretation of the references to color in this figure legend, the reader is referred to the web version of this article.)

aluminum and leads to a melt containing absorbed hydrogen. If the hydrogen solubility in the melt is reached (0.7 mL/100 g [6]), H_2 bubbles nucleate and diffuse through the melt pool up to the surface. However, they can be entrapped by the solidification front. Furthermore, the hydrogen solubility is approximatively 10 times larger in the liquid state than in the solid state [6]. With regard to this solubility shift, the solidified material could present pores rich in hydrogen or supersaturated solid solution. In the present case, the amount of hydrogen in the samples is 35 mL/100 g, i.e. 50 times the hydrogen solubility.

The second type of spherical defects is related to a high input of energy by the laser. Previous investigations have shown that an energy threshold exists beyond which unwished porosities appear [19–21]. This excess of energy brought to the system leads to instabilities within the melt pool and the active flow of the liquid metal traps some argon chamber gas. Kimura et al. [19] measured the gas composition of a bulk AlSi10Mg processed by SLM. An argon content of 67% was obtained for the highest energy density samples. At the opposite, for lower energy densities, Weingarten et al. [17] only observed 0.27% of argon in the voids of their samples.

Nevertheless, understanding the pore formation can not alone explain the heterogeneous distribution of porosity, i.e. almost all the porosities are observed in zone B of inclined struts. Since the porosities are preferentially located in the coarser microstructure zone B (DOZ), their nucleation could be justified by the difference in time spent at high temperature by both zones A and B. Based on the strut orientation of the lattice, two reasons can explain why zone B stays longer at high temperature than zone A.

Firstly, zone B cools down more slowly since it lays on powder (Fig. 1(b)). This lower cooling rate induces a higher local pre-heating in zone B for the next layer. Weingarten et al. [17] discussed the influence of the local pre-heating on the hydrogen pore formation by studying the evolution of bulk density with the scan break, i.e. the time between the end of one scan vector and the starting point of the following scan vector in bulk samples. This time dictates the temperature of the previously solidified part before building the upper layer. These previous researches showed that if the scan break decreases, the hydrogen pore density increases due to more local pre-heating of the following scan track. The lower cooling rate in zone B thus leads to a higher temperature of the material on which the next layer will be built. This should thus lead to a higher hydrogen pore density following the conclusions of Weingarten et al. [17]. Furthermore, this excess of energy in zone B due to its pre-heating leads to instabilities in the melt pool and argon pores may also form.

Secondly, zone B is preferentially affected by the successive laser tracks, i.e. the laser thermal penetration affects the previous solidified layers. Zone B thus sustains a heat treatment by the following laser scans. The assumed supersaturated metastable state can relax leading to pore formation and diffusion of the trapped hydrogen towards the existing cavities. Moreover, previous researches have shown that hydrogen solubility linearly increases with temperature (rise of ~0.69 mL/100 g for 100 °C [6]). Considering that zone B stays longer at high temperature, the amount of trapped hydrogen in this location potentially increases.

Fig. 2(b) exhibits the microstructure of a lattice strut after a T6 heat treatment, i.e. annealing at 525 °C for 5 h followed by water quenching (WQ) and artificial aging at 165 °C during 7 h [22]. The microstructure is completely homogeneous with a disappearance of visible melt pools as well as of distinct zones A and B. The Si rich eutectic is fully spheroidized and large Si rich precipitates are homogeneously distributed in the Al matrix. The hardness value after this T6 heat treatment is found to be 110 HV independently of the zone of analysis while 85.8 HV are measured after the sole solutionizing treatment (525 °C/5 h). Indeed, the 165 °C/7 h aging is expected to favor the formation of Mg_2Si age-hardening precipitates [22–23]. The observed microstructure coarsening is however the reason for the overall hardness decrease [22–23]. In agreement with literature [22], the present work shows a size of Si rich precipitates around 1.5 μm after annealing at 525 °C for 6 h.

To conclude, the effects of the building orientation of the struts on the microstructure of AlSi10Mg SLM lattice structures have been investigated. In the AlSi10Mg SLM as-built inclined strut, the upwards orientated part (zone A) is found to have a fine microstructure, a higher hardness in the melt pool and low porosity while the downwards orientated part (zone B) presents a coarse microstructure, a lower hardness with excessive porosities. Such excessive porosities are not observed in vertical struts. Since the amount of hydrogen detected in the samples is larger than the hydrogen solubility in the liquid melt pool (~0.7 mL/100 g), these voids are expected to be rich in hydrogen. The longer time spent at high temperature in the bottom part favors microstructure coarsening and hydrogen porosity growth. A T6 heat treatment leads to a slight hardness loss (~10 HV) due to Si precipitate growth and spheroidization. However, this heat treatment presents the advantage of suppressing all microstructure heterogeneities.

Acknowledgements

The authors acknowledge the financial support of the Interuniversity Attraction Poles Program from the Belgian State through the Belgian Policy agency, contract IAP7/21 INTEMATE. P. Delroisse acknowledges the financial support of the FRIA, Belgium. F. Hannard is acknowledged for helping in analyzing the tomography images and J. Adrien for acquiring these images.

References

[1] I. Maskery, N.T. Aboulkhair, A.O. Aremu, C.J. Tuck, I.A. Ashcroft, R.D. Wildman, R.J.M. Hague, Mater. Sci. Eng. A 670 (2016) 264–274.
[2] M.G. Rashed, M. Ashraf, R.A.W. Mines, P.J. Hazell, Mater. Des. 95 (2016) 518–533.
[3] E.O. Olakanmi, R.F. Cochrane, K.W. Dalgarno, Prog. Mater. Sci. 74 (2015) 401–477.
[4] W. Pei, W. Zhengying, C. Zhen, D. Jun, H. Yuyang, L. Junfeng, Z. Yatong, Appl. Surf. Sci. 408 (2017) 38–50.
[5] L. Thijs, K. Kempen, J.-P. Kruth, J. Van Humbeeck, Acta Mater. 61 (2013) 1809–1819.
[6] J.G. Kaufman, E.L. Rooy, Aluminum Alloy CastingsASM International 2004.
[7] I. Rosenthal, A. Stern, N. Frage, Metallogr. Microstruct. Anal. 3 (2014) 448–453.
[8] Y. Li, D. Gu, Mater. Des. 63 (2014) 856–867.
[9] N.T. Aboulkhair, N.M. Everitt, I. Ashcroft, C. Tuck, Addit. Manuf. 1 (2014) 77–86.
[10] W. Li, S. Li, J. Liu, A. Zhang, Y. Zhou, Q. Wei, C. Yan, Y. Shi, Mater. Sci. Eng. A 663 (2016) 116–125.
[11] L. Hitzler, C. Janousch, J. Schanz, M. Merkel, B. Heine, F. Mack, W. Hall, A. Öchsner, J. Mater. Process. Technol. 234 (2017) 48–61.
[12] C. Qiu, S. Yue, N.J.E. Adkins, M. Ward, H. Hassanin, P.D. Lee, P.J. Withers, M.M. Attallah, Mater. Sci. Eng. A 628 (2015) 188–197.
[13] M. Leary, M. Mazur, J. Elambasseril, M. McMillan, T. Chirent, Y. Sun, M. Qian, M. Easton, M. Brandt, Mater. Des. 98 (2016) 344–357.
[14] Struers, Application Notes, 2008.
[15] J.-Y. Buffiere, E. Maire, J. Adrien, J.-P. Masse, E. Boller, Exp. Mech. 50 (2010) 289–305.
[16] M. Suard, G. Martin, P. Lhuissier, R. Dendievel, F. Vignat, J.-J. Blandin, F. Villeneuve, Addit. Manuf. 8 (2015) 124–131.
[17] C. Weingarten, D. Buchbinder, N. Pirch, W. Meiners, K. Wissenbach, R. Poprawe, J. Mater. Process. Technol. 221 (2015) 112–120.
[18] X.P. Li, K.M. O'Donnell, T.B. Sercombe, Addit. Manuf. 10 (2016) 10–14.
[19] T. Kimura, T. Nakamoto, Mater. Des. 89 (2016) 1294–1301.
[20] N. Read, W. Wang, K. Essa, M.M. Attallah, Mater. Des. 65 (2015) 417–424.
[21] N.T. Aboulkhair, I. Maskery, C. Tuck, I. Ashcroft, N.M. Everitt, J. Mater. Process. Technol. 230 (2016) 88–98.
[22] N.T. Aboulkhair, C. Tuck, I. Ashcroft, I. Maskery, N.M. Everitt, Metall. Mater. Trans. A 46 (2015) 3337–3341.
[23] G.A. Edwards, K. Stiller, G.L. Dunlop, M.J. Couper, Acta Mater. 46 (1998) 3893–3904.